JACS
JOURNAL OF THE AMERICAN CHEMICAL SOCIETY

Communication

pubs.acs.org/JACS

Efficient Water Oxidation Using CoMnP Nanoparticles

Da Li, Habib Baydoun, Cláudio N. Verani, and Stephanie L. Brock*

Department of Chemistry, Wayne State University, Detroit, Michigan 48202, United States

Supporting Information

ABSTRACT: The development of efficient water oxidation catalysts based on inexpensive and Earth-abundant materials is a prerequisite to enabling water splitting as a feasible source of alternative energy. In this work, we report the synthesis of ternary cobalt manganese phosphide nanoparticles from the solution-phase reaction of manganese and cobalt carbonyl complexes with trioctylphosphine. The CoMnP nanoparticles (ca. 5 nm in diameter) are nearly monodisperse and homogeneous in nature. These CoMnP nanoparticles are capable of catalyzing water oxidation at an overpotential of 0.33 V with a 96% Faradaic efficiency when deposited as an ink with carbon black and Nafion. A slight decrease in activity is observed after 500 cycles, which is ascribed to the etching of P into solution, as well as the oxidation of the surface of the nanoparticles. Manganese-based ternary phosphides represent a promising new system to explore for water oxidation catalysis.

Splitting water into hydrogen and oxygen represents an ideal source of clean renewable energy.[1] However, water oxidation ($2H_2O \rightarrow O_2 + 4H^+ + 4e^-$) – the first step in the overall water splitting reaction – has a high activation barrier that coupled with the need for transfer of four electrons and four protons, presents a bottleneck in the transformation of water into O_2 and H_2.

Ruthenium and iridium oxides are well-known water oxidation catalysts.[2,3] Nevertheless, the scarcity of Ru and Ir pose serious limitations to the widespread adoption of water splitting as a green approach to renewable energy. To address this problem, research has been focused on the synthesis of novel materials composed of stable, Earth-abundant metals capable of efficient catalytic water oxidation. Inspired by the oxygen-evolving center of Photosystem II, manganese-based materials (oxides and phosphates) have garnered considerable attention as water oxidation catalysts.[4−8]

At the same time, transition metal phosphide nanoparticles are emerging as a new class of water oxidation catalysts with reports of high activity in Ni_2P,[9,10] CoP,[11−15] and CoFeP.[16,17] While manganese-based phosphides may appear to be natural catalyst candidates, such materials have yet to be investigated. This gap is at least in part due to a lack of synthetic methodologies for manganese phosphide nanoparticles.

We have previously reported the synthesis of MnP nanoparticles.[18] However, attempts to use these particles as water oxidation catalysts revealed that MnP is not stable under oxidizing conditions, which we attribute to the highly oxophilic nature of manganese. As shown in Figure S1, the presence of a broad irreversible preoxidation peak at ~1.4 V_{RHE} is observed in the first oxidation sweep. The following sweeps revealed a large drop in the current density consistent with an irreversible oxidative transformation of MnP during water oxidation. Accordingly, we sought to moderate the activity of Mn by the inclusion of a second metal, namely, cobalt. In this paper, we report on a simple and highly reproducible route for the synthesis of novel cobalt manganese phosphide, CoMnP, nanoparticles and the investigation of their catalytic behavior toward water oxidation.

The initial target of our investigation was the phase $Co_{0.5}Mn_{0.5}P$, which we expected to be feasibly attained as discrete nanoparticles based on the facts that (1) MnP and CoP are isostructural and (2) it is possible to synthesize the entire solid solution by solid-state methods in the bulk phase.[19−21] Adapting known methods for MnP and CoP nanoparticle synthesis, we injected $Co_2(CO)_8$ and $Mn_2(CO)_{10}$ into a solution of hot 1-octadecene and oleylamine, followed by injection of trioctylphosphine (TOP) and elevation of the solution temperature to 350 °C (see Supporting Information, SI, for details). However, the X-ray diffraction (XRD) pattern of the product showed that the peaks correspond to orthorhombic CoMnP and not to the expected $Co_{0.5}Mn_{0.5}P$ phase (Figure 1a), and this is confirmed by SAED (Figure S3).

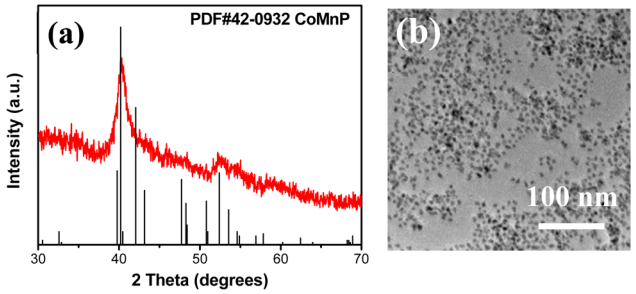

Figure 1. Powder XRD (a) and TEM (b) of CoMnP nanoparticles. The reference pattern for CoMnP (PDF # 42-0932) is shown.

Intriguingly, we have not been successful preparing the Mn_2P phase (the Mn end-product of $Co_{1-x}Mn_xP$), producing only MnP or no isolable product. We hypothesize that incorporating Co favors the inclusion of low-valent Mn, thus facilitating the formation of the "M_2P" phase. Transmission electron microscopy (TEM) images reveal the formation of spherical nanoparticles with an average diameter of 4.59 ± 0.76 nm (Figures 1b, S2). The corresponding energy dispersive X-ray

Received: February 10, 2016
Published: March 13, 2016

DOI: 10.1021/jacs.6b01543
J. Am. Chem. Soc. 2016, 138, 4006−4009

spectrum (EDX, Figure S3) indicates that the atomic ratio of Co, Mn, and P is close to 1:1:1.3. The composition of the nanoparticles was further confirmed from inductively coupled plasma-mass spectrometry (ICP-MS) measurements which show a ratio of Co/Mn/P of 1:1:1.1 (Figure S3). The slight excess of P is attributed to the presence of residual TOP as surface binding groups.

The homogeneous nature of the synthesized nanoparticles was verified by performing scanning transmission electron microscopy (STEM) measurements combined with elemental mapping and line scans (Figures 2, S4). The data show that Co, Mn, and P are homogeneously distributed within the nanoparticles, thus suggesting the formation of a solid solution.

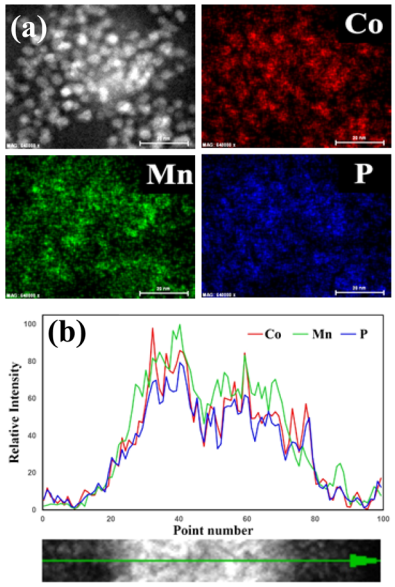

Figure 2. STEM image and elemental mapping data (a), and line scan compositional data (b) of CoMnP nanoparticles. Co is shown in red, Mn in green, and P in blue.

On the basis of prior work with CoFeP, which exhibits higher activity than the corresponding ternary oxide or the binary Co or Fe phosphide materials,[16] $CoMnO_2$ and Co_2P nanoparticles were prepared for comparison to CoMnP (loading: 0.284 mg/cm^2, see SI for details; Figure S5). The catalytic behavior of the different nanoparticles was determined by preparing an ink composed of the nanoparticles, carbon black and Nafion (details in SI). The overpotential, defined as the potential by which the current density reaches 10 mA/cm^2, is commonly used as a figure of merit for heterogeneous water oxidation catalysts.[2,22] For CoMnP, the overpotential was 0.33 V at a current density of 10 mA/cm^2 (Figures 3, S6). This overpotential places the CoMnP catalyst among the top tier of water oxidation catalysts, and on par with iridium oxide (Table S1).[2,8−14,16,17,23,24] For comparison, Co_2P nanoparticles showed a higher overpotential of 0.37 V and the overpotential of $CoMnO_2$ was higher still at 0.39 V. The Tafel plots in Figure 3b are derived from the polarization curves, and they show the plots of overpotential vs the log of the current density. While the $CoMnO_2$ and the Co_2P have a Tafel slope of 95 and 128 mV/dec, respectively, CoMnP has a slope of 61 mV/dec, close to the ideal value of 59 mV/dec (equivalent to $2.3RT/F$) associated with a one-electron transfer prior to the rate-limiting step.[25,26]

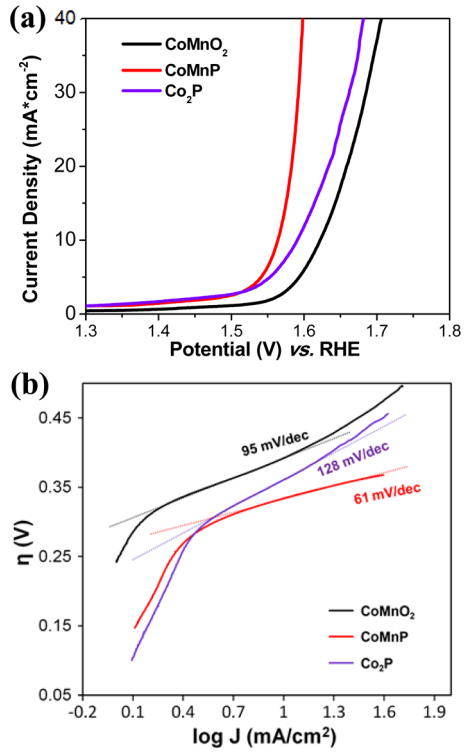

Figure 3. (a) Polarization curves for nanoparticles of CoMnP, $CoMnO_2$, and Co_2P in 1.0 M KOH; (b) Tafel plots derived from the polarization curves.

The decrease in overpotential for CoMnP relative to Co_2P is attributed to synergism between the two metal centers. It has been suggested that the insertion of a second metal may help lower the thermodynamic barrier of a proton-coupled electron transfer (PCET) pre-equilibrium while facilitating O−O bond formation, leading to enhanced catalytic activity.[25] Most proposed mechanisms for CoO_x species suggest the need the formation of vicinal high-valent oxo species.[25,27−29] While the formation of Co═O is energetically demanding and the product is unstable, the formation of Mn═O species is relatively facile.[30] As such it is expected that the presence of an Mn center in close proximity to a Co center would lower the activation barrier needed for catalysis, thus explaining the decrease in overpotential in CoMnP compared to Co_2P. Likewise, we posit that the high oxophilicity of Mn is moderated by Co, facilitating catalyst turnover. The lower activation barrier of phosphides over oxides is likely due to the intrinsic electric conductivity of the phosphides relative to corresponding oxides. These reaction barrier variations appear to lead to distinct mechanisms in the three materials, as reflected in the widely different Tafel slopes. Further investigation will be necessary to ascertain the validity of these suggestions.

Faradaic efficiency was determined by performing a controlled potential electrolysis (CPE) experiment using an airtight H-type cell, and analyzing the head space gas by gas chromatography (details in SI, Figure S7). The experimentally determined oxygen quantity was compared to the expected amount of oxygen based on the charge consumed. The Faradaic efficiency reached 96% after 10 h of catalysis.

The stability of the materials under catalytic conditions was determined by collecting polarization curves between 1.03 and 2.23 V (vs RHE) over 500 cycles. Upon cycling, an increase in

DOI: 10.1021/jacs.6b01543
J. Am. Chem. Soc. 2016, 138, 4006−4009

the overpotential was observed from 0.33 to 0.37 V (Figure 4). Interestingly, after intermediate cycling (200 cycles), the

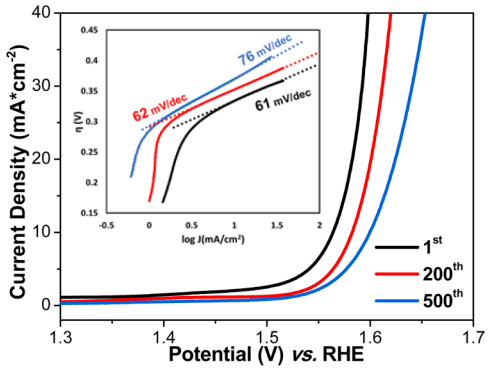

Figure 4. Polarization curves for CoMnP nanoparticles, in 1.0 M KOH initially (black), after 200 (red) and 500 CV sweeps (blue) vs RHE. Inset: Tafel plots derived from the cycling experiments.

overpotential increased to 0.35 V, which was accompanied by a nominal increase in the Tafel slope (Figure 4, inset). However, after continued cycling (500 cycles, Figure S8), the Tafel slope increased to 76 mV/dec. These observations suggest that as the catalyst is cycled, the nature of the catalyst, and consequently the mechanism of operation, is changing.

In an effort to understand the deactivation, we performed X-ray photoelectron spectroscopy (XPS) analysis on the samples before and after a 10 h CPE experiment (Figure 5, Figure S9).

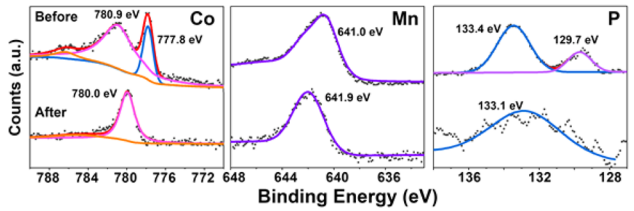

Figure 5. High-resolution XPS patterns for CoMnP nanoparticles before (top) and after (bottom) electrolysis for 10 h: Co ($2p_{3/2}$), Mn ($2p_{3/2}$), and P ($2p_{3/2}$).

Before catalysis, the high resolution XPS spectrum of Co ($2p_{3/2}$) comprises a peak at 777.8 eV assigned to the binding energy of Co in Co_2P,[31] the Co^{2+} peaks at 780.9 eV, as well as a satellite peak (787.1 eV), corresponding to CoO, which presumably formed due to surface oxidation. The XPS spectrum of Mn ($2p_{3/2}$) exhibited a peak at 641.0 eV, corresponding to oxidized manganese species such as MnO or Mn_2O_3. The absence of low-valent Mn peaks in the spectrum is attributed to the high oxophicility of Mn, resulting in surface oxide formation.[32] The XPS spectrum of P ($2p_{3/2}$) showed two peaks assigned to phosphide at 129.7 eV and phosphate or phosphite (PO_x or P−O species) at 133.4 eV. In contrast, the high-resolution XPS patterns of Co, Mn, and P after catalytic cycling show the disappearance of low energy peaks of Co (777.8 eV) and P (129.7 eV), as well as a shift toward higher binding energies for Mn (from 641.0 to 641.9 eV). These observations are in accordance with nanoparticle surface oxidation during the catalytic process to form MPO_x and MO_x species and are in line with recent reports in which Ni_2P nanomaterials were oxidized during the course of the water oxidation reaction to form NiO_x and phosphate species.[9,10] Moreover, the P signal after catalytic cycling appears very weak (barely discernible above the noise level, Figure 5), suggesting that the surface-bound phosphates are being etched. To probe the possibility of leaching during catalysis, ICP-MS analysis was performed on a solution following a 15-h CPE experiment (Figure S10, Table S2). The results show the presence of Co, Mn, and P in solution with a ratio of 1:7:234, thus suggesting that P is leaching into solution at a significant rate, whereas metal leaching is marginal with Mn dominating Co. Because surface-bound phosphates have been reported to mediate water oxidation via proton-coupled electron transfer,[5] the loss of surface phosphate combined with metal oxidation may account for the decrease in activity and shift in the mechanism.

In conclusion, we have reported on the successful synthesis of homogeneous, nearly monodisperse CoMnP nanoparticles. This new material is an active and efficient water oxidation catalyst that can operate at an overpotential of 0.33 V and 96% Faradaic efficiency. After 500 cycles, the overpotential for catalysis increased to 0.37 V, likely due to surface oxidation and phosphorus etching from the nanoparticles. Evaluation of the efficacy of phosphate buffers for stabilization, as well as studies on compositional effects, is underway.

■ ASSOCIATED CONTENT

Supporting Information

The Supporting Information is available free of charge on the ACS Publications website at DOI: 10.1021/jacs.6b01543.

Detailed experimental descriptions, material characterization, as well as sample calculations (PDF)

■ AUTHOR INFORMATION

Corresponding Author

*sbrock@chem.wayne.edu

Notes

The authors declare no competing financial interest.

■ ACKNOWLEDGMENTS

This work is supported by the National Science Foundation under Grant Nos. CHE-1367702 and DMR-1361470 for S.L.B. and CHE-1500201 for C.N.V. and by the U.S. Department of Energy, Office of Science, Office of Basic Energy Sciences under the Grant No. DE-SC0001907 for C.N.V. Both D.L. and H.B. acknowledge Rumble Fellowship Awards from Wayne State University. TEM data were acquired on a JEOL 2010 TEM with funds provided by NSF MRI award 0216084. TEM, ICP-MS and powder X-ray diffraction were acquired in the Lumigen Instrument Center, Wayne State University. We thank S. Trimpin for use of the RDE, Z. Mei for assistance with TEM, K. Sun for XPS and Y. Liu for data acquired on the FEI Titan STEM.

■ REFERENCES

(1) Lewis, N. S.; Nocera, D. G. *Proc. Natl. Acad. Sci. U. S. A.* **2007**, *104*, 20142.

(2) McCrory, C. C. L.; Jung, S.; Peters, J. C.; Jaramillo, T. F. *J. Am. Chem. Soc.* **2013**, *135*, 16977.

(3) Frame, F. A.; Townsend, T. K.; Chamousis, R. L.; Sabio, E. M.; Dittrich, T.; Browning, N. D.; Osterloh, F. E. *J. Am. Chem. Soc.* **2011**, *133*, 7264.

(4) Jeong, D.; Jin, K.; Jerng, S. E.; Seo, H.; Kim, D.; Nahm, S. H.; Kim, S. H.; Nam, K. T. *ACS Catal.* **2015**, *5*, 4624.

DOI: 10.1021/jacs.6b01543
J. Am. Chem. Soc. 2016, 138, 4006−4009

(5) Jin, K.; Park, J.; Lee, J.; Yang, K. D.; Pradhan, G. K.; Sim, U.; Jeong, D.; Jang, H. L.; Park, S.; Kim, D.; Sung, N. E.; Kim, S. H.; Han, S.; Nam, K. T. *J. Am. Chem. Soc.* **2014**, *136*, 7435.
(6) Jin, K.; Chu, A.; Park, J.; Jeong, D.; Jerng, S. E.; Sim, U.; Jeong, H. Y.; Lee, C. W.; Park, Y. S.; Yang, K. D.; Pradhan, G. K.; Kim, D.; Sung, N. E.; Kim, S. H.; Nam, K. T. *Sci. Rep.* **2015**, *5*, 10279.
(7) Kuo, C. H.; Mosa, I. M.; Poyraz, A. S.; Biswas, S.; E-Sawy, A. M.; Song, W. Q.; Luo, Z.; Chen, S. Y.; Rusling, J. F.; He, J.; Suib, S. L. *ACS Catal.* **2015**, *5*, 1693.
(8) Liang, Y. Y.; Wang, H. L.; Zhou, J. G.; Li, Y. G.; Wang, J.; Regier, T.; Dai, H. J. *J. Am. Chem. Soc.* **2012**, *134*, 3517.
(9) Han, A.; Chen, H. L.; Sun, Z. J.; Xu, J.; Du, P. W. *Chem. Commun.* **2015**, *51*, 11626.
(10) Stern, L.-A.; Feng, L.; Song, F.; Hu, X. *Energy Environ. Sci.* **2015**, *8*, 2347.
(11) Chang, J.; Xiao, Y.; Xiao, M.; Ge, J.; Liu, C.; Xing, W. *ACS Catal.* **2015**, *5*, 6874.
(12) Wang, P.; Song, F.; Amal, R.; Ng, Y. H.; Hu, X. *ChemSusChem* **2016**, *9*, 472.
(13) Liu, M.; Li, J. *ACS Appl. Mater. Interfaces* **2016**, *8*, 2158.
(14) Hou, C.-C.; Cao, S.; Fu, W.-F.; Chen, Y. *ACS Appl. Mater. Interfaces* **2015**, *7*, 28412.
(15) Surówka, J.; Budniok, A.; Bzowski, B. e.; Warczewski, J. *Thin Solid Films* **1997**, *307*, 233.
(16) Mendoza-Garcia, A.; Zhu, H. Y.; Yu, Y. S.; Li, Q.; Zhou, L.; Su, D.; Kramer, M. J.; Sun, S. H. *Angew. Chem., Int. Ed.* **2015**, *54*, 9642.
(17) Mendoza-Garcia, A.; Su, D.; Sun, S. *Nanoscale* **2016**, *8*, 3244.
(18) Gregg, K. A.; Perera, S. C.; Lawes, G.; Shinozaki, S.; Brock, S. L. *Chem. Mater.* **2006**, *18*, 879.
(19) Fjellvag, H.; Kjekshus, A. *Acta Chem. Scand.* **1984**, *38*, 563.
(20) Fujii, S.; Ishida, S.; Asano, S. *J. Phys. F: Met. Phys.* **1988**, *18*, 971.
(21) Grosvenor, A. P.; Cavell, R. G.; Mar, A. *J. Solid State Chem.* **2007**, *180*, 2702.
(22) Jung, S.; McCrory, C. C. L.; Ferrer, I. M.; Peters, J. C.; Jaramillo, T. F. *J. Mater. Chem. A* **2016**, *4*, 3068.
(23) Fominykh, K.; Feckl, J. M.; Sicklinger, J.; Doblinger, M.; Bocklein, S.; Ziegler, J.; Peter, L.; Rathousky, J.; Scheidt, E. W.; Bein, T.; Fattakhova-Rohlfing, D. *Adv. Funct. Mater.* **2014**, *24*, 3123.
(24) Ryu, J.; Jung, N.; Jang, J. H.; Kim, H. J.; Yoo, S. J. *ACS Catal.* **2015**, *5*, 4066.
(25) Surendranath, Y.; Kanan, M. W.; Nocera, D. G. *J. Am. Chem. Soc.* **2010**, *132*, 16501.
(26) Gileadi, E. *Electrode Kinetics for Chemists, Chemical Engineers and Materials Scientists*; Wiley-VCH: New York, 1993; pp 127−184.
(27) Zhang, M.; de Respinis, M.; Frei, H. *Nat. Chem.* **2014**, *6*, 362.
(28) Gerken, J. B.; McAlpin, J. G.; Chen, J. Y. C.; Rigsby, M. L.; Casey, W. H.; Britt, R. D.; Stahl, S. S. *J. Am. Chem. Soc.* **2011**, *133*, 14431.
(29) Kärkäs, M. D.; Verho, O.; Johnston, E. V.; Åkermark, B. *Chem. Rev.* **2014**, *114*, 11863.
(30) Winkler, J. R.; Gray, H. B. In *Molecular Electronic Structures of Transition Metal Complexes I*; Mingos, D. M. P., Day, P., Dahl, J. P., Eds.; Springer: New York, 2012; Vol. *142*, p 17.
(31) Blanchard, P. E. R.; Grosvenor, A. P.; Cavell, R. G.; Mar, A. *Chem. Mater.* **2008**, *20*, 7081.
(32) Colson, A. C.; Whitmire, K. H. *Chem. Mater.* **2011**, *23*, 3731.

DOI: 10.1021/jacs.6b01543
J. Am. Chem. Soc. 2016, 138, 4006−4009